Opto-Electronic Advances

CN 51–1781/TN ISSN 2096–4579 (Print) ISSN 2097–3993 (Online)

Finely regulated luminescent Ag-In-Ga-S quantum dots with green-red dual emission toward white light-emitting diodes

Zhi Wu, Leimeng Xu, Jindi Wang and Jizhong Song

Citation: Wu Z, Xu LM, Wang JD, et al. Finely regulated luminescent Ag-In-Ga-S quantum dots with green-red dual emission toward white light-emitting diodes. *Opto-Electron Adv* **7**, 240050(2024).

https://doi.org/10.29026/oea.2024.240050

Received: 2 March 2024; Accepted: 22 July 2024; Published online: 18 September 2024

Related articles

Luminescence regulation of Sb^{3+} in 0D hybrid metal halides by hydrogen bond network for optical anti-counterfeiting

Dehai Liang, Saif M. H. Qaid, Xin Yang, Shuangyi Zhao, Binbin Luo, Wensi Cai, Qingkai Qian, Zhigang Zang

Opto-Electronic Advances 2024 **7**, 230197 doi: 10.29026/oea.2024.230197

Highly enhanced UV absorption and light emission of monolayer WS_2 through hybridization with Ti_2N MXene quantum dots and g-C_3N_4 quantum dots

Anir S. Sharbirin, Rebekah E. Kong, Wendy B. Mato, Trang Thu Tran, Eunji Lee, Jolene W. P. Khor, Afrizal L. Fadli, Jeongyong Kim

Opto-Electronic Advances 2024 **7**, 240029 doi: 10.29026/oea.2024.240029

Opto-Electronic Advances

Article

September 2024, Vol. 7, No. 9

DOI: 10.29026/oea.2024.240050

Finely regulated luminescent Ag-In-Ga-S quantum dots with green-red dual emission toward white light-emitting diodes

Zhi Wu, Leimeng Xu*, Jindi Wang and Jizhong Song*

Ag-In-Ga-S (AIGS) quantum dots (QDs) have recently attracted great interests due to the outstanding optical properties and eco-friendly components, which are considered as an alternative replacement for toxic Pb- and Cd-based QDs. However, enormous attention has been paid to how to narrow their broadband spectra, ignoring the application advantages of the broadband emission. In this work, the AIGS QDs with controllable broad green-red dual-emission are first reported, which is achieved through adjusting the size distribution of QDs by controlling the nucleation and growth of AIGS crystals. Resultantly, the AIGS QDs exhibit broad dual-emission at green- and red- band evidenced by photoluminescence (PL) spectra, and the PL relative intensity and peak position can be finely adjusted. Furthermore, the dual-emission is the intrinsic characteristics from the difference in confinement effect of large particles and tiny particles confirmed by temperature-dependent PL spectra. Accordingly, the AIGS QDs (the size consists of 17 nm and 3.7 nm) with 530 nm and 630 nm emission could successfully be synthesized at 220 °C. By combining the blue light-emitting diode (LED) chips and dual-emission AIGS QDs, the constructed white light-emitting devices (WLEDs) exhibit a continuous and broad spectrum like natural sunlight with the Commission Internationale de l'Eclairage (CIE) chromaticity coordinates of (0.33, 0.31), a correlated color temperature (CCT) of 5425 K, color rendering index (CRI) of 90, and luminous efficacy of radiation (LER) of 129 lm/W, which indicates that the AIGS QDs have huge potential for lighting applications.

Keywords: quantum dots; Ag-In-Ga-S; dual emission; white light-emitting diodes

Wu Z, Xu LM, Wang JD et al. Finely regulated luminescent Ag-In-Ga-S quantum dots with green-red dual emission toward white light-emitting diodes. *Opto-Electron Adv* **7**, 240050 (2024).

Introduction

Colloidal semiconductor quantum dots (QDs) have drawn much attention due to their size-dependent tunable bandgap, high color saturation, which exhibit great advantages in the application of lightings and displays[1,2]. Recent years, some outstanding QDs, such as CdSe and perovskite QDs have achieved extraordinary development, but the use of toxic Cd and Pb has limited their further application. Thus, exploring novel semiconductor QDs with environmentally components and prominent luminescence properties are highly desired. Ternary Ⅰ-Ⅲ-$Ⅵ_2$ alloyed compounds (I = Cu, Ag; III = Ga, In; VI = S, Se, Te)[3–6] are widely investigated. Cu-based ternary QDs feature a broad emission peak and low quantum efficiency due to their intrinsic band structure and defect-related luminescence[7,8]. Recently, Ag-In-Ga-S (AIGS) QDs, which exhibit controllable light emission in almost full visible range and higher photoluminescence

Key Laboratory of Materials Physics of Ministry of Education, Laboratory of Zhongyuan Light, School of Physics, Zhengzhou University, Daxue Road 75, Zhengzhou 450052, China.

*Correspondence: LM Xu, E-mail: xuleimeng@zzu.edu.cn; JZ Song, E-mail: songjizhong@zzu.edu.cn

Received: 2 March 2024; Accepted: 22 July 2024; Published online: 18 September 2024

quantum yield (PLQY), have shown great potential in lightings and displays[9–17]. Compared with the classical Cd-based system, the AIGS QDs feature a wider emission in visible range, accompanied by a main peak of strong bandgap luminescence and a weak peak from defect luminescence. Currently, great efforts such as formation of core-shell structure[18–29] and surface ligand treatment[30–32], have been devoted to improving the main peak, suppressing defect peaks, and thus narrowing photoluminescence (PL) spectra to meet the needs of high-definition displays. While the feature of broadband emission also has great advantages in phosphor-converted lightings and is ignored[33–36].

The emission peaks of the low energy region in dual-spectral emission AIGS QDs are mainly caused by band-edge or lattice defects[31,32]. As a result, the luminous intensity of this peak is relatively weak and cannot be controlled, making it impossible to achieve high-quality lighting applications. In order to effectively regulate the luminous intensity of the low-energy region, we have studied the nucleation and growth processes of QDs in the synthesis process, and this is largely related to the effect of temperature on quantum size.

Based on the quantum size effect, the band gap and luminous wavelength of QDs can be adjusted through controlling the size, morphology or structure[29]. The size dependent band gap follows the Bruce equation:

$$\Delta E\,(R) = E_{\mathrm{g}}\,(R) + \frac{h^2}{8R^2}\left(\frac{1}{m_{\mathrm{e}}^*} + \frac{1}{m_{\mathrm{h}}^*}\right)\frac{-1.8e^2}{4\pi\varepsilon_0\varepsilon_\alpha R}\ ,$$

where ΔE is defined as the size-dependent bandgap due to quantum effects, E_{g} is the bandgap of the bulk materials, R is the radius of QDs, $m_{\mathrm{e}}{}^*$ is the effective mass of electron, $m_{\mathrm{h}}{}^*$ is the effective mass of hole, ε_0 is the dielectric constant in vacuum, ε_α is the effective constant of electron, e is the electron charge. Based on above formula, the motion of electrons and holes in QDs will be limited with decreasing size, leading to the increase in kinetic energy. The increased kinetic energy will result in the larger energy gap and blue shift in spectra, as shown in Scheme 1. Benefitting from the quantum size effect of QD materials, rich and tunable spectra can be obtained by controlling the size of QD crystals[37]. Through controlling the crystal nucleation and growth properly, QDs with two distinct size distribution (large and tiny particles) exhibit the dual broadband emission, which are beneficial for the manufacture of white light devices (WLEDs). The WLED is generally composed of blue chips and yellow or green+red phosphors[38–40]. Compared to traditional rare earth phosphors, the one component AIGS QDs with dual-emission at green (≈530 nm) and red (≈630 nm), large Stokes' shifts, eco-friendly composites and facile solution synthesis process, exhibit great potential in WLEDs.

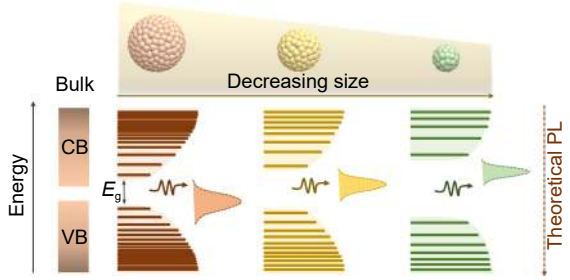

Scheme 1 | Schematic diagram of the size-dependent band gap and spectral correspondence based on size effect of QDs.

In this work, the AIGS QDs with dual-emission are obtained through one-pot synthesis, and the controlled bimodal PL spectra is reported for the first time. The dual-emissive PL is achieved through adjusting the crystalline size and composition of AIGS QDs, the nucleation and growth of which can be controlled by regulating the growth temperature. Resultantly, the PL of dual-emission at 530 nm and 630 nm is realized, and the relative intensity of the two peaks can be adjusted. Furthermore, the intrinsic emission characteristics of the dual-emissive PL is demonstrated through PL measurements under different excitation wavelength and temperature. Possessing green- and red-emission simultaneously, this QDs exhibit great advantages in WLEDs. Through combing the dual-missive QDs with blue-emitting chips, a white light-emitting diode is obtained, which exhibit tunable color temperature and CIE chromaticity coordinates.

Experimental section

Chemicals. Silver acetate (AgOAc, 99.5%), indium triacetate ($In(OAc)_3$, 99.99%), gallium nitrate hydrate ($Ga(NO_3)_3$, 99.9%), sodium diethyldithiocarbamate (NaDDTC, 98%), 1-dodecanethiol (DDT, 98%), n-hexane (GC), oleylamine (OAm) were purchased from Macklin, low-density polyethylene (LDPE) was purchased from Dongguan Huachuang Plastic Raw Material Firm. Methanol (AR) was purchased from Fuyu Reagent. Trichloromethane (AR) was purchased from Luoyang Chemical Factory.

Synthesis of Gallium Diethyldithiocarbamate ($Ga(DDTC)_3$). $Ga(DDTC)_3$ was prepared following the previous report with some modifications[30], where the volume was expanded and the purification process was optimized. Typically, a 200 mL 0.3 mol/L NaDDTC (10.2756 g) aqueous solution was added dropwise to a 200 mL 0.1 mol/L $Ga(NO_3)_3$ (5.1148 g) aqueous solution with continuous stirring at atmospheric environment for 3 h. The collection was filtered through the suction filter device and repeat washing three times to achieve purity. Then the white powder was obtained after drying in vacuum oven at 60 °C overnight.

Synthesis of AIGS QDs. The synthesis process was modified from reported method[30], where the volume was expanded and reaction temperature was optimized. Typically, AgOAc (0.4 mmol, 66.8 mg), $In(OAc)_3$ (0.8 mmol, 232 mg) and $Ga(DDTC)_3$ (0.8 mmol, 268 mg) were dissolved in OAm (20 mL) in a three-necked flask. The mixture solution was evacuated at 100 °C for 30 min. Then, the temperature was heated to 180 °C, 190 °C, 200 °C, 210 °C, 220 °C, 230 °C, 240 °C or 250 °C, respectively under nitrogen (N_2) flow and maintained for 30 min. Subsequently, 0.5 mL of dodecanethiol was injected for a further 30 min. After cooling to room temperature, the nanoparticle portion was isolated by precipitation with trichloromethane (2 mL) and methanol (8 mL). The solution was centrifuged three times (10,000 rpm, 1 min), and dispersed in hexane (1 mL).

Construction of AIGS QD-based white light-emitting diodes. 100 μL of QDs were added to 5 g of thermoplastic polymer powder (LDPE), followed by 0.1 g of photo-dispersible powder. After mixing with a stirrer for 3 min, the mixture was processed into a yellow film by hot pressing. According to the principle of three primary colours, the yellow quantum dot film was superimposed on a blue LED chip (455 nm) to obtain a white light emitting device.

Material characterization. The steady-state photoluminescence (PL) spectra and photoluminescence excitation (PLE) spectra were studied through a spectrofluorometer (Hitachi Fluorescence Spectrophotometer F-4700). The Ultraviolet–visible (UV-vis) absorption spectrum was measured using a UV-vis spectrophotometer (Hitachi UV-Visible/NIR Spectrophotometer UH5700). The QD morphologies were observed using a transmission electron micros-copy (TEM) instrument (Hitachi, H-7650) at an acceleration voltage of 100 kV, whereas high-resolution TEM (HRTEM) images were obtained using a 200 kV TEM (JEOL, JEM-2100). Powder X-ray diffraction (XRD) analysis was performed using an X-ray diffractometer (Rigaku, SmartLab) equipped with a parallel beam/parallel slit analyzer. The chemical composition of the QDs was determined using an inductively coupled plasma atomic emission spectrometer (Shimadzu, ICPS-7510). Variable temperature PL spectrum are measured using a FLS1000 Photoluminescence Spectrometer (Cryo77, Tianjin Orient-KOJI Instrument and TAP-02, Tianjin Orient-KOJI Instrument). Variable power PL spectrum are used by a laser diode controller (ADR-1805).

Results and discussion

The AIGS QDs are synthesized through the modified hot-injection method from previous report[30], where the varied temperature is used to regulate the size of the quantum dots. Through controlling the reaction temperature, AIGS QDs with different size distributions are obtained, as shown in Fig. 1(a–c) and Fig. S1. When reacting at 180 °C, QDs exhibit spherical particles with an average diameter of 16.5 nm (Fig. 1(a) and 1(e)). Increasing the reaction temperature to 220 °C, a mass of tiny QDs within 5 nm appear, and the average diameter of these small particles is 3.7 nm (Fig. 1(b) and 1(g)). As the temperature rises further to 250 °C, the synthesized QDs are almost tiny particles with an average diameter of 3.7 nm (Fig. 1(c) and 1(i)). The corresponding HRTEM images of QDs are presented in Fig. 1(d, f) and 1(h), all these particles reveal well-ordered lattice fringes, which means these QDs show a uniformly single crystalline characteristic. And the *d*-spacing is corresponding to (112) plane of tetragonal phase, which is consistent with previous reports[28,30]. It should be noted that the large particles and small particles have the same crystal plane spacing, which indicates they possess the same crystal structure. It will be further confirmed in later XRD discussion.

Due to the variation in dimension, QDs grow at different temperature exhibit tunable light emission, their corresponding typical spectra are shown in Fig. 1(j–l). QDs with large particles possess red light emission (Fig. 1(j)), with the appearance of the small particles, the green-emitting band of PL spectra occur (Fig. 1(l)), which is consistent with the quantum confinement effect of QDs. Through controlling the nucleation and growth, QDs with large and small particles can be obtained, leading to the realization of QDs with dual-emission (Fig. 1(k)).

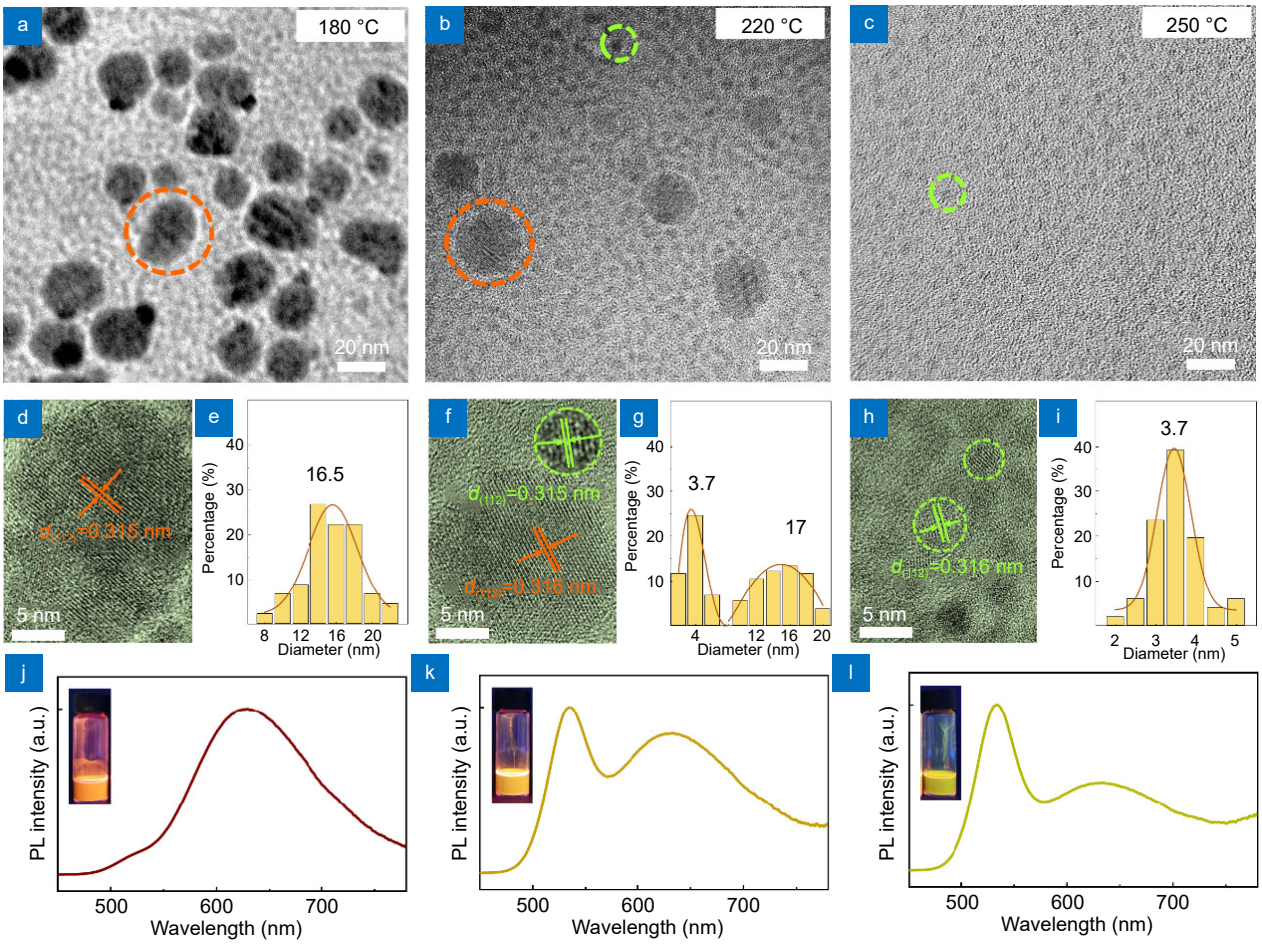

Fig. 1 | The temperature-dependent microstructure of AIGS QDs and corresponding PL spectra. (**a**, **b**, **c**) TEM, (**d**, **f**, **h**) HRTEM images, (**e**, **g**, **i**) histograms of the statistical distributions of particle sizes and corresponding (**j**, **k**, **l**) normalized PL spectra of the AIGS QDs synthesized at 180 °C, 220 °C and 250 °C, respectively.

The nucleation and growth controlling mechanism and of AIGS QDs and the fine regulation of spectra will be further explained in the following content.

The schematic diagram of temperature-affected nucleation and growth is presented in Fig. 2(a). For the liquid-phase synthesis process of colloidal QDs, homogeneous nucleation occurs when supersaturation of the precursor molecules is sufficient to overcome the nucleation barrier. The higher the supersaturation, the higher the nucleation probability and the smaller the critical nucleus[2,41]. When reacting at lower temperature (180 °C), the reactive activity of precursors is not fully mobilized, leading to low nucleation rate. The nucleuses lager than the critical size can continue to grow, while the clusters smaller than the critical size will dissolve, the dissolved ions tend to grow on the as-formed crystal core, resulting in large grains. With the temperature rises, the more intense molecular motion and the increased supersaturation is favorable for efficient nucleation[42], leading to smaller particles. Through regulating the reaction temperature, the AIGS QDs simultaneously containing large and small particles can be obtained, which exhibit dual emission as presented in Fig. 1(k).

The crystalline structure of the AIGS QDs are further analyzed through XRD as shown in Fig. 2(b), all the AIGS QDs obtained at different temperature exhibit tetragonal phase, the appearance of characteristic peaks at 26.7°, 45.5°, and 53° are located between the positions of (112), (204), and (312) planes for $AgGaS_2$ (PDF #25-0351) and $AgInS_2$ (PDF #23-1330), which is consistent with previous reports[28,30]. While the QDs synthesized at lower temperature (180 °C) exhibit impurity phase due to the incomplete reaction caused by low activity of precursor. Furthermore, the atomic metrology of the QDs are measured via inductively coupled plasma emission spectroscopy (ICP-OES), the QDs have similar atomic ratio that is close to the composition of Ag-(In/Ga)-S_2 (Fig. 2(c) and Table S1), except the QDs obtained at the

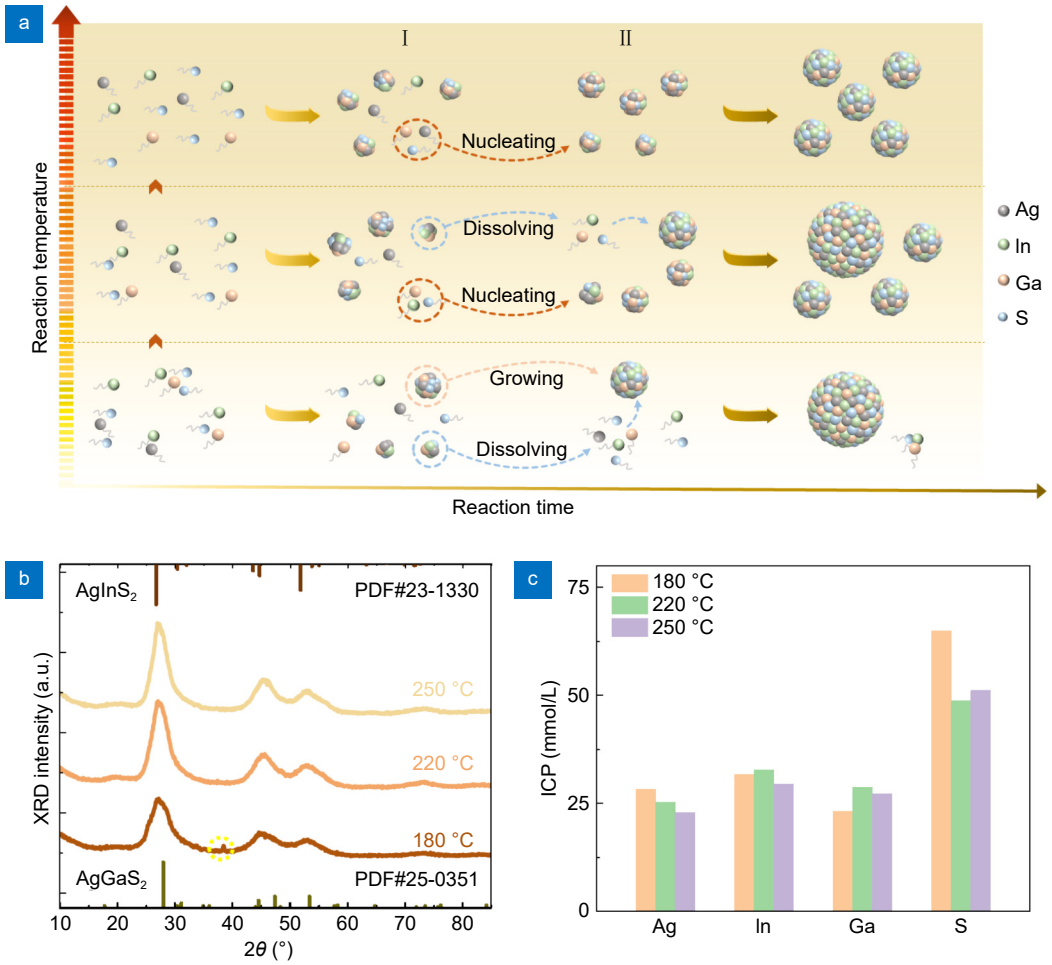

Fig. 2 | The growth mechanism of dual-emissive AIGS QDs. (**a**) Schematic diagram of nucleation and growth patterns as a function of temperature. Stage Ⅰ: increased temperature induces decreased critical size and more nucleation, stage Ⅱ: higher nucleation rate at higher temperature lead to the growth of smaller crystals under the same concentration of precursor compared to lower temperature. (**b**) XRD patterns of the AIGS QDs synthesized at 180 °C, 220 °C and 250 °C, inserted on the upper and lower axe are the standard diffraction peaks of $AgInS_2$ and $AgGaS_2$. (**c**) The element ratio of the AIGS QDs synthesized at 180 °C, 220 °C and 250 °C analyzed by ICP-OES.

lower temperature due to the unreacted metal precursor salt. Above results indicate that the large and small particles have the same structure not the heterogeneous phase, which also demonstrates that the dual emission is due to the size effect rather than different phases.

The microstructure of the typical dual emissive AIGS QDs is further demonstrated. The schematic diagram of the tetragonal AIGS is shown in Fig. 3(a). And Fig. 3(b–f) present the EDS element mapping of typical AIGS QDs containing large and small particles obtained at 230 °C. It can be seen that Ag, In, Ga, S are evenly distributed on all the selected grains, which further supports above conclusion that the QDs with large and small sizes have the same composition and structure.

Based on above adjustment of crystal size, the spectra of QDs can be finely controlled. Figure 4(a, b) presents the photographs and corresponding spectra of the AIGS QDs synthesized at different temperature. At lower temperature (180 °C, 190 °C), the QDs exhibit broadband emission with the peak at 630 nm, which is derived from the large-sized AIGS QDs. With the temperature increasing (200 °C, 210 °C), a new small peak at green band appear that is due to the generation of small-sized particles in the system. As the temperature continues to rise (220 °C, 230 °C), the green-band emission is also enhanced on account of the increased small-sized particles, the QDs with dual emission are obtained. When the temperature is further increased (240 °C, 250 °C), the red-band emission weakened to almost disappear. Correspondingly, the optical photographs under UV irradiation also shows the change from red emission to green emission. In addition, the peak position of the dual emission can also be adjusted

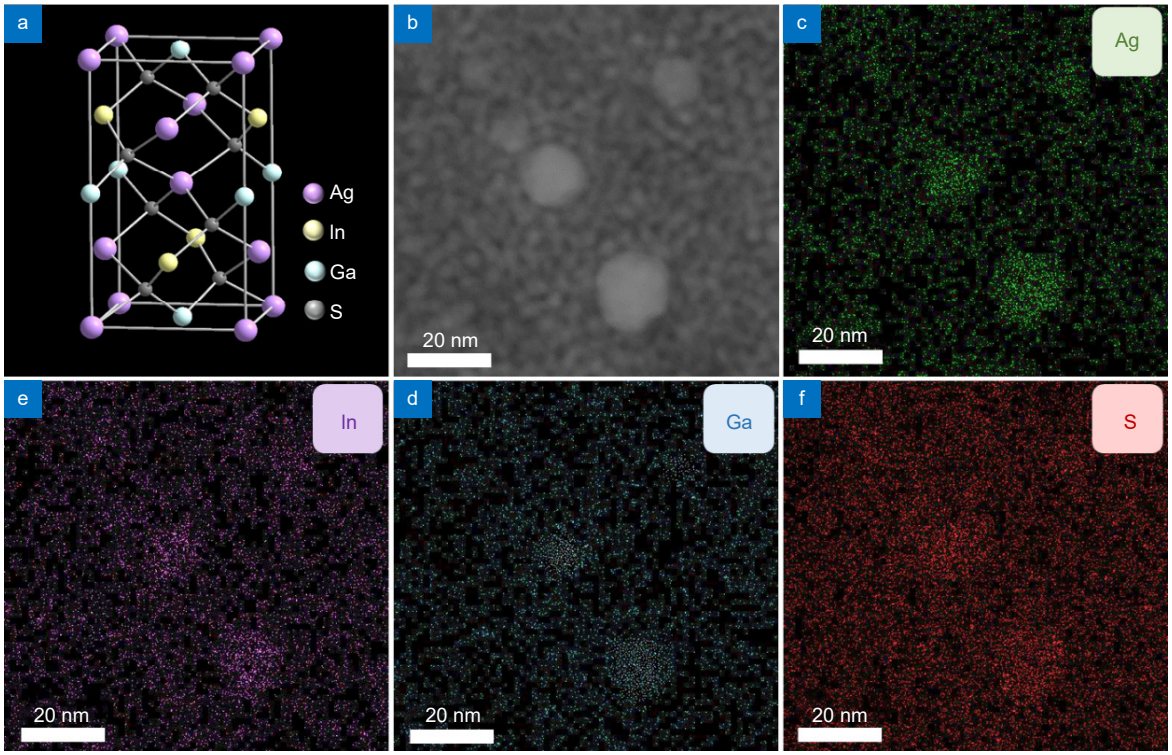

Fig. 3 | The element distribution of typical AIGS QDs. (**a**) Schematic diagram structure of AIGS. (**b–f**) EDS element mapping of typical AIGS QDs for (c) Ag, (d) In, (e) Ga, (f) S.

through regulating the proportion of Ga/In as shown in Fig. S2, the overall blue shift of the spectra is observed with increasing Ga that is consistent with previous reported result[9–17]. The AIGS QDs have large Stoker shift the absorption band edge of which is at 480 nm (dash line in Fig. 4(b)), this character makes it advantageous for lighting applications.

To further prove that the feature of this dual emission is derived from intrinsic luminescence of QDs, the temperature-, power- and excitation wavelength-dependent PL are measured, as shown in Figs. 5, S4. As can be seen from Figs. 5(a, b), S3, with the increasing temperature from 80 K to 380 K, both PL peaks of the dual emission redshift slightly due to the lattice expansion, but no new fluorescence peaks occur[43–45]. The stable existence of both emission peaks at low temperature when the phonon energy is suppressed, and the peak positions are almost the same as those at room temperature, indicating that the luminescence is derived from the intrinsic emission of AIGS QDs. The PL intensity increase with the decreasing temperature due to suppression of non-radiative pathways at lower temperature. And the narrower full width at half maximum (FWHM) is due to the reduced probability of non-radiative recombination caused by lattice vibration declines with decreasing temperature[46].

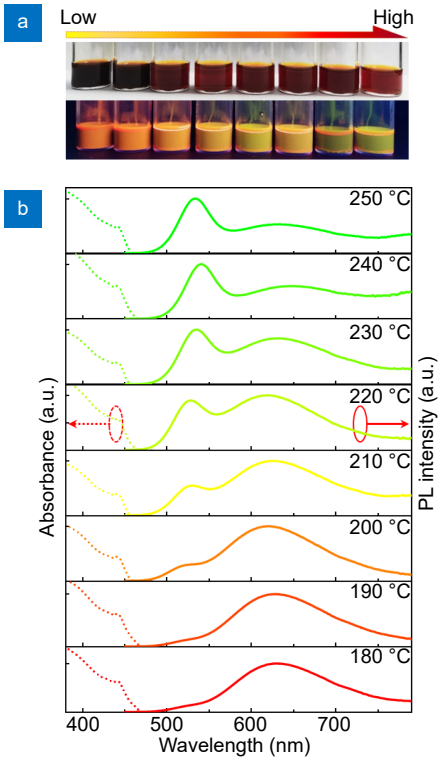

Fig. 4 | The optical properties of AIGS QDs with dual emission. (**a**) Photographs of the AIGS QDs synthesized at different temperature under room light (top) and UV irradiation (bottom). (**b**) Corresponding PL and UV-vis absorbance spectra were recorded with the excitation wavelength of 365 nm under different temperature.

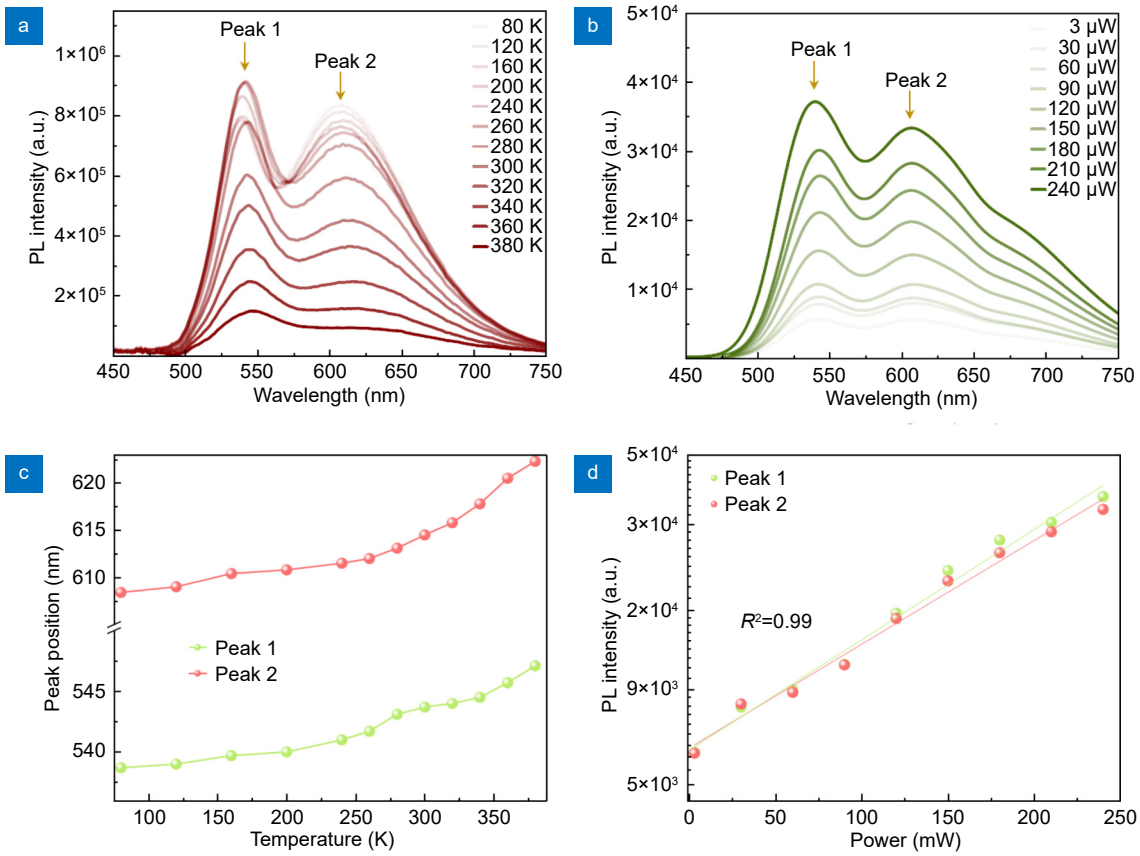

Fig. 5 | PL mechanism of dual-emissive AIGS QDs. (**a**) The temperature-dependent PL spectra of AIGS QDs under 370 nm laser excitation. (**b**) Peak position versus temperature for AIGS QDs. (**c**) Excitation power (370 nm)-dependent PL spectra AIGS QDs. (**d**) Emission intensity versus excitation power for the AIGS QDs at room temperature.

In addition, the power-dependent-PL spectra under 370 nm excitation are shown in Fig. 5(c) and 5(d), R^2 is a fitting parameter. R^2 = 0.99, the results show that the emission intensity of AIGS quantum dots has a good linear correlation with the excitation power, also indicating that the dual emission is due to the grain size and do not arise from other defects[47]. Moreover, the PL spectra of the dual-emissive AIGS QDs under different excitation wavelength are also tested (Fig. S4), and the emission peak did not shift and the PL spectra shape did not change. Above analysis demonstrated that the characteristic peaks are derived from intrinsic exciton emission. Through regulating the size and components of AIGS QDs, the relative intensity of the dual-emissive peaks as well as the peak position can be controlled. The stability of AIGS QDs are also tested (Fig. S5), The AIGS QDs maintain 89% of original PL intensity after storing in atmosphere for six months, and maintain 63% of original PL intensity after continuous UV irradiation for 24 h, which exhibit good stability.

Benefiting from the AIGS QDs with tunable broad dual-emission and good stability, the white light-emitting diodes can be constructed on blue chips using only one material, without the need to mix multiple phosphors. To build the white-emitting device, an appropriate amount of AIGS QDs are mixed with thermoplastic polymer powders (LDPE, low-density polyethylene), and then processed into films through thermo-compression formation, the white-emitting device is obtained by combining blue LED chip (455 nm) (Fig. 6(a)). The bright and pure white-emission can be observed from the photograph. The emission spectra and the CIE color coordinate of the as-prepared WLED at 6.30–6.48 V are delineated in Fig. 6(b) and 6(c). With the increasing voltage, the PL intensity of the device enhances and the color temperature changes from cold to warm white light, which is due to the increasing red band induced by particle aggregation under increased light irradiation. The electroluminescent (EL) spectrum covers a broad region from 400 to 780 nm. The WLED exhibits a continuous and broad spectrum like natural sunlight with the CIE chromaticity coordinates of (0.33, 0.31), a CCT of 5425

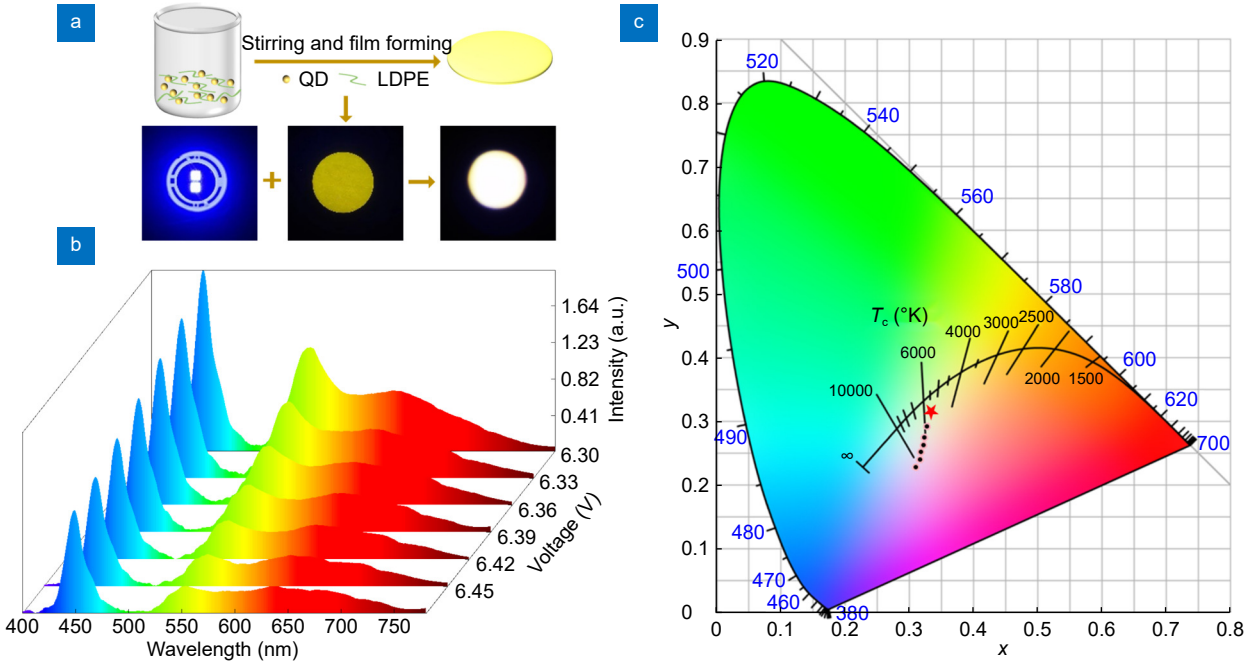

Fig. 6 | WLED based on dual-emissive AIGS QDs. (**a**) The schematic diagram of constructing dual-emissive AIGS QD-based white light-emitting diode and the corresponding optical photograph of the white-emitting device. (**b**) PL spectra of the WLED and (**c**) corresponding CIE chromaticity coordinates under different voltage.

K, CRI of 90, and LER of 129 lm/W at a drive current of 6.30 V. Furthermore, the operation stability of the constructed WLEDs is tested at 1200 cd/m^2, T_{50} of the device is 6.5 h, as shown in Fig. S6.

Conclusion

In conclusion, we propose a finely regulated luminescent AIGS QDs with dual emission through controlling the crystal size of QDs. The relative intensity of bimodal PL and peak position can be regulated by adjusting the size distribution and composition of AIGS QDs. And the single phase of the dual-emissive QDs is demonstrated from the crystalline structure and component analysis. The typical sample exhibits yellow luminescence with broad dual emission at 530 nm and 630 nm respectively, furthermore, the intrinsic emission characteristics of the dual-emission is analyzed by the PL under different temperature, power and excitation wavelength. Taking advantage of the spectral property, the AIGS QDs are mixed with thermoplastic polymer to form emitting film via thermo-compression process. By combining the blue LED chips and dual-emission AIGS QDs, a WLED with a CIE color coordinate of (0.30, 0.31), a CCT of 5425 K, CRI of 90, and LER of 129 lm/W is successfully fabricated. In a short, the dual-emissive AIGS QDs indicating the potential for practical application.

References

1. Murray CB, Norris DJ, Bawendi MG. Synthesis and characterization of nearly monodisperse CdE (E = sulfur, selenium, tellurium) semiconductor nanocrystallites. *J Am Chem Soc* **115**, 8706–8715 (1993).
2. Sun CJ, Jiang YZ, Zhang L et al. Toward the controlled synthesis of lead halide perovskite nanocrystals. *ACS Nano* **17**, 17600–17609 (2023).
3. Hamanaka Y, Ogawa T, Tsuzuki M et al. Photoluminescence properties and its origin of $AgInS_2$ quantum dots with chalcopyrite structure. *J Phys Chem C* **115**, 1786–1792 (2011).
4. Jain S, Bharti S, Bhullar GK et al. I-III-VI core/shell QDs: synthesis, characterizations and applications. *J Lumin* **219**, 116912 (2020).
5. Zhang J, Zeng B, Ye HH et al. Facile synthesis of ternary $AgInS_2$ nanowires and their self-assembly of fingerprint-like nanostructures. *Chin Chem Lett* **32**, 1507–1510 (2021).
6. Azhniuk Y, Lopushanska B, Selyshchev O et al. Synthesis and optical properties of Ag-Ga-S quantum dots. *Phys Status Solidi B* **259**, 2100349 (2022).
7. Suzuki K, Kuzuya T, Hamanaka Y. Luminescence enhancement in $CuInS_2$ nanoparticles through the selective passivation of nonradiative recombination sites by phosphine ligands. *J Phys Chem C* **126**, 16751–16758 (2022).
8. Zang HD, Li HB, Makarov NS et al. Thick-shell $CuInS_2$/ZnS quantum dots with suppressed “blinking” and narrow single-particle emission line widths. *Nano Lett* **17**, 1787–1795 (2017).
9. Uematsu T, Doi T, Torimoto T et al. Preparation of luminescent $AgInS_2$-$AgGaS_2$ solid solution nanoparticles and their optical properties. *J Phys Chem Lett* **1**, 3283–3287 (2010).
10. Kameyama T, Yamauchi H, Yamamoto T et al. Tailored photoluminescence properties of Ag(In, Ga)Se_2 quantum dots for near-

infrared *in vivo* imaging. *ACS Appl Nano Mater* **3**, 3275–3287 (2020).
11. Liu ZY, Guan ZY, Li X et al. Rational design and synthesis of highly luminescent multinary Cu-In-Zn-S semiconductor nanocrystals with tailored nanostructures. *Adv Opt Mater* **8**, 1901555 (2020).
12. Rismaningsih N, Yamauchi H, Kameyama T et al. Controlling electronic energy structure of Ag-In-Ga-S-Se quantum dots showing band-edge emission. *Meet Abstr* **MA2020-02**, 3121 (2020).
13. Guan ZY, Ye HH, Lv PW et al. The formation process of five-component Cu-In-Zn-Se-S nanocrystals from ternary Cu–In–S and quaternary Cu-In-Se-S nanocrystals via gradually induced synthesis. *J Mater Chem C* **9**, 8537–8544 (2021).
14. Rismaningsih N, Yamauchi H, Kameyama T et al. Photoluminescence properties of quinary Ag-(In, Ga)-(S, Se) quantum dots with a gradient alloy structure for *in vivo* bioimaging. *J Mater Chem C* **9**, 12791–12801 (2021).
15. Kottayi R, Ilangovan V, Sittaramane R. Wide light-harvesting $AgZnGaS_3$ quantum dots as an efficient sensitizer for solar cells. *Opt Mater* **134**, 113036 (2022).
16. Xie XL, Zhao JX, Lin OY et al. Narrow-bandwidth blue-emitting Ag-Ga-Zn-S semiconductor nanocrystals for quantum-dot light-emitting diodes. *J Phys Chem Lett* **13**, 11857–11863 (2022).
17. Kameyama T, Kishi M, Miyamae C et al. Wavelength-tunable band-edge photoluminescence of nonstoichiometric Ag-In-S nanoparticles via Ga^{3+} doping. *ACS Appl Mater Interfaces* **10**, 42844–42855 (2018).
18. Li JB, Wang LW. First principle study of core/shell structure quantum dots. *Appl Phys Lett* **84**, 3648–3650 (2004).
19. Reiss P, Protière M, Li L. Core/shell semiconductor nanocrystals. *Small* **5**, 154–168 (2009).
20. Raevskaya A, Lesnyak V, Haubold D et al. A fine size selection of brightly luminescent water-soluble Ag-In-S and Ag-In-S/ZnS quantum dots. *J Phys Chem C* **121**, 9032–9042 (2017).
21. Uematsu T, Wajima K, Sharma DK et al. Narrow band-edge photoluminescence from AgInS2 semiconductor nanoparticles by the formation of amorphous III-VI semiconductor shells. *NPG Asia Mater* **10**, 713–726 (2018).
22. Hoisang W, Uematsu T, Yamamoto T et al. Core nanoparticle engineering for narrower and more intense band-edge emission from $AgInS_2/GaS_x$ core/shell quantum Dots. *Nanomaterials* **9**, 1763 (2019).
23. Bai TY, Wang XM, Dong YY et al. One-pot synthesis of high-quality AgGaS2/ZnS-based photoluminescent nanocrystals with widely tunable band gap. *Inorg Chem* **59**, 5975–5982 (2020).
24. Motomura G, Ogura K, Iwasaki Y et al. Electroluminescence from band-edge-emitting $AgInS_2/GaS_x$ core/shell quantum dots. *Appl Phys Lett* **117**, 091101 (2020).
25. Wei JH, Li F, Chang C et al. Synthesis of emission tunable $AgInS_2$/ZnS quantum dots and application for light emitting diodes. *J Phys Commun* **4**, 045016 (2020).
26. Li X, Tong X, Yue S et al. Rational design of colloidal $AgGaS_2$/CdSeS core/shell quantum dots for solar energy conversion and light detection. *Nano Energy* **89**, 106392 (2021).
27. Lee SJ, Lee JE, Lee CJ et al. Design of Ag-Ga-$S_{2-x}Se_x$-based eco-friendly core/shell quantum dots for narrow full-width at half-maximum using noble $ZnGa_2S_4$ shell material. *J Korean Phys Soc* **81**, 935–941 (2022).
28. Lee HJ, Im S, Jung D et al. Coherent heteroepitaxial growth of I-III-VI_2 Ag(In, Ga)S_2 colloidal nanocrystals with near-unity quantum yield for use in luminescent solar concentrators. *Nat Commun* **14**, 3779 (2023).
29. Motomura G, Uematsu T, Kuwabata S et al. Quantum-dot light-emitting diodes exhibiting narrow-spectrum green electroluminescence by using Ag-In-Ga-S/GaS_x quantum dotS. *ACS Appl Mater Interfaces* **15**, 8336–8344 (2023).
30. Hoisang W, Uematsu T, Torimoto T et al. Luminescent quaternary $Ag(In_xGa_{1-x})S_2/GaS_y$ core/shell quantum dots prepared using dithiocarbamate compounds and photoluminescence recovery via post treatment. *Inorg Chem* **60**, 13101–13109 (2021).
31. Hoisang W, Uematsu T, Torimoto T et al. Surface ligand chemistry on quaternary $Ag(In_xGa_{1-x})S_2$ semiconductor quantum dots for improving photoluminescence properties. *Nanoscale Adv* **4**, 849–857 (2022).
32. Uematsu T, Tepakidareekul M, Hirano T et al. Facile high-yield synthesis of Ag-In-Ga-S quaternary quantum dots and coating with gallium sulfide shells for narrow band-edge emission. *Chem Mater* **35**, 1094–1106 (2023).
33. Chen JW, Xiang HY, Wang J et al. Perovskite white light emitting diodes: progress, challenges, and opportunities. *ACS Nano* **15**, 17150–17174 (2021).
34. Huang GX, Huang Y, Liu ZL et al. White light-emitting diodes based on quaternary Ag-In-Ga-S quantum dots and their influences on melatonin suppression index. *J Lumin* **233**, 117903 (2021).
35. Lu HX, Hu Z, Zhou WJ et al. Synthesis and structure design of I-III-VI quantum dots for white light-emitting diodes. *Mater Chem Front* **6**, 418–429 (2022).
36. Hu Z, Lu HX, Zhou WJ et al. Aqueous synthesis of 79% efficient AgInGaS/ZnS quantum dots for extremely high color rendering white light-emitting diodes. *J Mater Sci Technol* **134**, 189–196 (2023).
37. Omata T, Nose K, Otsuka-Yao-Matsuo S. Size dependent optical band gap of ternary I-III-VI_2 semiconductor nanocrystals. *J Appl Phys* **105**, 073106 (2009).
38. Zhu PF, Thapa S, Zhu HY et al. Solid-state white light-emitting diodes based on 3D-printed $CsPbX_3$-resin color conversion layers. *ACS Appl Electron Mater* **5**, 5316–5324 (2023).
39. Zhu PF, Thapa S, Zhu HY et al. Composition engineering of lead-free double perovskites towards efficient warm white light emission for health and well-being. *J Alloys Compd* **960**, 170836 (2023).
40. Zhang KS, Fan WX, Yao TL et al. Polymer‐surface‐mediated mechanochemical reaction for rapid and scalable manufacture of perovskite QD phosphors. *Adv Mater* **36**, 2310521 (2024).
41. Thanh NTK, Maclean N, Mahiddine S. Mechanisms of nucleation and growth of nanoparticles in solution. *Chem Rev* **114**, 7610–7630 (2014).
42. Zhao HF, Zhu YC, Ye HY et al. Atomic‐scale structure dynamics of nanocrystals revealed by in situ and environmental transmission electron microscopy. *Adv Mater* **35**, 2206911 (2023).
43. Sun GW, Liu XY, Liu Z et al. Emission wavelength tuning via competing lattice expansion and octahedral tilting for efficient red perovskite light‐emitting diodes. *Adv Funct Mater* **31**, 2106691 (2021).
44. Wang PH, Tang JL, Kang YB et al. Crystal structure and optical properties of GaAs nanowires. *Acta Phys Sin* **68**, 087803 (2019).
45. Jiang B, Chen SL, Cui XL et al. Temperature-dependent photo-

luminescence in hybrid iodine-based perovskites film. *Acta Phys Sin* **68**, 246801 (2019).

46. Huang HL, Yang YL, Qiao SY et al. Accommodative organoammonium cations in a - sites of Sb-In halide perovskite derivatives for tailoring BroadBand photoluminescence with X - ray scintillation and white - light emission. *Adv Funct Mater* **34**, 2309112 (2024).
47. Zhou R, Sui LZ, Liu XB et al. Multiphoton excited singlet/triplet mixed self-trapped exciton emission. *Nat Commun* **14**, 1310 (2023).

Acknowledgements

This work is supported by National Natural Science Foundation of China (Grant Nos. 52272166, 22205214, and 12204427).

Author contributions

J. Z. Song conceived the idea, designed the experimental data. Z. Wu were involved in the experiment preparation, test experiments. L. M. Xu analyzed the data. All authors contributed to discussions and finalization of the manuscript.

Competing interests

The authors declare no competing financial interests.

Supplementary information

Supplementary information for this paper is available at https://doi.org/10.29026/oea.2024.240050